THE JOURNAL OF BIOLOGICAL CHEMISTRY VOL. 283, NO. 49, pp. 34069–34075, December 5, 2008

Crystal Structure of Filamentous Aggregates of Human DJ-1 Formed in an Inorganic Phosphate-dependent Manner*

Received for publication, June 3, 2008, and in revised form, October 1, 2008 Published, JBC Papers in Press, October 14, 2008, DOI 10.1074/jbc.M804243200

Sun-Shin Cha[‡1], Ha Il Jung[‡§], Hyesung Jeon[¶], Young Jun An[‡§], In-Kwon Kim[‖], Sanguk Yun[**], Hyun Jin Ahn[‡‡], Kwang Chul Chung[‡‡], Sang Hee Lee[§], Pann-Ghill Suh[**], and Sa-Ouk Kang[‖2]

From the [‡]Marine and Extreme Genome Research Center, Korea Ocean Research & Development Institute, Ansan 426-744, Republic of Korea, the [¶]Korea Institute of Science and Technology, Seoul 130-650, Republic of Korea, the [‖]School of Biological Sciences, Seoul National University, Seoul 151-742, Republic of Korea, the [**]Department of Life Science, POSTECH, Pohang 790-784, Republic of Korea, the [§]Department of Biological Sciences, Myongji University, Yongin 449-728, Republic of Korea, and the [‡‡]Department of Biology, Yonsei University, Seoul 120-749, Republic of Korea

Mutations in the *DJ-1* gene have been implicated in the autosomal recessive early onset parkinsonism. DJ-1 is a soluble dimeric protein with critical roles in response to oxidative stress and in neuronal maintenance. However, several lines of evidence suggest the existence of a nonfunctional aggregated form of DJ-1 in the brain of patients with some neurodegenerative diseases. Here, we show that inorganic phosphate, an important anion that exhibits elevated levels in patients with Parkinson disease, transforms DJ-1 into filamentous aggregates. According to the 2.4-Å crystal structure, DJ-1 dimers are linearly stacked through P_i-mediated interactions to form protofilaments, which are then bundled into a filamentous assembly.

Human DJ-1 is a 189-amino acid, homo-dimeric protein. It was first identified as a novel candidate for the oncogene product that transformed mouse NIH3T3 cells in concert with activated *ras* (1). After this initial identification, DJ-1 has been shown to have various physiological implications. DJ-1 was characterized as a protein that regulates an RNA-protein interaction (2) and positively modulates the androgen receptor (3). In addition to functions in somatic cells, DJ-1 seems to play roles in male fertility. CAP-1, or SP22, a rat homologue of DJ-1, has been identified as a key protein related to infertility observed in male rats that were exposed to sperm toxicants (4–6). DJ-1 began to attract attention after a homozygous deletion in the *DJ-1* gene was revealed to be responsible for the autosomal recessive early onset Parkinson disease (PD)[3] (7). Like the deletion mutation, several missense mutations of the *DJ-1* gene found in inherited PD cases also appear to cause a complete lack of DJ-1 function. For example, the L166P mutation appears to destabilize the dimeric structure of DJ-1 by promoting the unfolding of its C-terminal region, subsequently enhancing its degradation via the proteasome system and leading to the loss of DJ-1 in cells (8–10).

Accumulating evidence reveals that DJ-1 plays protective functions against oxidative stress. DJ-1 is a molecular chaperone (11) that is activated in an oxidative cytoplasmic environment (12). Activated DJ-1 inhibits α-synuclein aggregation, the major component of Lewy bodies, which are the characteristic intracytoplasmic neuronal inclusions in PD and are closely associated with the progression of PD. DJ-1 also acts as a redox-sensitive negative regulator of apoptosis. DJ-1 contributes to the activation of the PI3K/Akt survival signaling pathway (13, 14) and blocks the Daxx-ASK1 proapoptotic pathway by sequestering Daxx from ASK1 (15). Studies using mice and *Drosophila* also suggest that DJ-1 plays critical roles in cell survival and response to oxidative stress (13, 16–20).

Structural alterations of DJ-1 are closely associated with its functions. Thus far, three structural modifications of the DJ-1 dimeric structure have been reported. First, DJ-1 is sumoylated at lysine residue 130 by PIASxα. Proper sumoylation is thought to be essential in *ras*-dependent cellular transformation, cell growth promotion, and anti-UV-induced apoptosis (21). Second, a cysteine residue (Cys^{106}) of DJ-1 is oxidized to sulfinic acid under oxidative stress conditions (11, 22), which causes a relocalization of DJ-1 to mitochondria. In addition, a C106A mutant fails to prevent cell death against oxidative stress, indicating the importance of oxidation at Cys^{106} for DJ-1 function (22, 23). Third, the solubility of DJ-1 is altered to form insoluble aggregates in brains of patients with neurodegenerative diseases (24–29). DJ-1 colocalizes with tau-positive inclusions over a range of neurodegenerative tauopathies, including Alzheimer disease, and with α-synuclein-positive glial inclusions in multiple system atrophy (24, 25, 29). In addition, insoluble DJ-1 is dramatically increased in brains of sporadic PD patients (28, 29). These findings suggest that abnormal aggregation of DJ-1 may be involved in the pathogenesis of multiple neurodegenerative diseases. Here, we report biochemical and structural investigations of DJ-1 aggregates formed in a P_i-dependent manner.

* This work was supported by the Functional Proteomics Center Program, Korea Ministry of Science and Technology and by the Marine & Extreme Genome Research Center Program, Ministry of Land, Transport, and Maritime Affairs, Republic of Korea. This work was also supported by Korea Institute of Science and Technology institutional grants and a Research Fellowship of the BK21 Project, Republic of Korea (to I. K. K.). The costs of publication of this article were defrayed in part by the payment of page charges. This article must therefore be hereby marked "*advertisement*" in accordance with 18 U.S.C. Section 1734 solely to indicate this fact.

The atomic coordinates and structure factors (code 3BWE) have been deposited in the Protein Data Bank, Research Collaboratory for Structural Bioinformatics, Rutgers University, New Brunswick, NJ (http://www.rcsb.org/).

[1] To whom correspondence may be addressed. E-mail: chajung@kordi.re.kr.

[2] To whom correspondence may be addressed. E-mail: kangsaou@snu.ac.kr.

[3] The abbreviations used are: PD, Parkinson disease; EM, electron micrograph(s).

EXPERIMENTAL PROCEDURES

Purification of DJ-1—The DJ-1 gene (encoding residues 1–189) was amplified, inserted into pET-21a (Novagen) and introduced into *Escherichia coli* strain B834 (DE3), and tDJ-1 was purified as described (11). For purification of pDJ-1, the cells were grown to an A_{600} of ~0.7 in Luria-Bertani medium containing 0.1 mg/ml ampicillin at 37 °C, and the expression of DJ-1 was induced by 1 mM isopropyl-β-D-thiogalactoside. After 4-h induction at 37 °C, the cells were harvested and resuspended in sodium phosphate buffers (pH 7.5) containing 1 mM dithiothreitol. The cells were disrupted by sonication, and the cell debris was discarded by centrifugation. The supernatants were loaded on a nickel-nitrilotriacetic acid column (Novagen) and eluted with sodium phosphate butters containing 20 mM imidazole. The eluted fraction was loaded on a Q-Sepharose Fast Flow column (Amersham Biosciences) and eluted with a 0–1 M NaCl gradient in sodium phosphate buffers (pH 7.5) containing 1 mM dithiothreitol.

Dynamic Light Scattering—Measurements were taken at 22 °C using a DynaPro instrument (Protein Solutions Inc.) equipped with a thermostatted cell. DJ-1 in 20 mM Tris buffer, pH 7.5 (tDJ-1), and DJ-1 in sodium phosphate, pH 7.5 (pDJ-1), at concentrations of 1 mg/ml were centrifuged at 14,000 rpm for 10 min at 4 °C. 60 μl of the supernatants were added to the cuvette, and the light scattering intensity was collected 30 times at an angle of 90° using a 10-s acquisition time. Data analyses were performed using the Dynapro V.5 software.

Circular Dichroism—CD experiments were performed on a Jasco J-810 spectropolarimeter using a 0.2-cm-path length cell, with a 1-nm bandwidth and a 4-s response time. Near-UV CD spectra were collected from 340 to 240 nm with a scan speed of 50 nm/min and 1-nm step resolution. Five individual scans were added and averaged.

Electron Microscopy—Purified pDJ-1 in a phosphate buffer condition was diluted and sampled 1 and 3 days after purification. pDJ-1 (0.6 mg/ml) was applied to carbon-coated grids and negatively stained with 2% uranyl acetate. The samples were visualized on a Philips CM30 electron microscope using a TVIPS FastScan-F114T CCD camera at a 47,000× magnification.

Crystallization, Data Collection, Model Building, and Refinement—The crystals of pDJ-1 were obtained by vapor diffusion from droplets containing 2 μl of protein solution plus 2 μl of precipitant solution containing 2 M ammonium sulfate, 0.4 M sodium potassium tartrate, and 0.1 M sodium cacodylate, pH 6.5, which were equilibrated against 0.5 ml of the same precipitant solution at 277 K. For data collection, the crystals were frozen at −170 °C using a cryostream cooler (Oxford Cryosystems) after a brief immersion in a cryoprotectant solution containing 20% glycerol in the same mother liquor. A 2.4 Å data set was collected at beamline 5A of the Photon Factory (Table 1). The data were integrated and scaled using HKL2000. The crystal structure of DJ-1 was determined by molecular replacement using AMoRe. Refinement was done with a maximum likelihood algorithm implemented in CNS program (Table 1). Molecular graphic manipulations were performed with QUANTA software (Molecular Simulations Inc., San Diego, CA.). After completing the adjustment of side chains according to electron density, the model was subjected to a positional refinement, causing the *R* value to decrease to 27.2%. At this stage, water molecules were added using the X-solvate utility of QUANTA, and P_i was incorporated into the corresponding density. The subsequent refinement and manual refitting of model reduced *R* and R_{free} values to 23.4 and 28.7%, respectively. The ideality of the model stereochemistry was verified by PROCHECK. The Ramachandran plot indicates 90.1% of nonglycine, and nonproline residues are in the most favored regions in the final model.

TABLE 1
Summary of crystallographic analysis

Data collection	
Space group	*C*2
Unit cell (Å)	$a = 193.62$, $b = 102.58$, $c = 85.54$, $\beta = 113.7°$
Wavelength (Å)	1.12714
Resolution (Å)	50-2.4
R_{sym} (%)[a,b]	8.1 (34)
Average I/σ	16.5 (4.7)
Completeness (≥3σ) (%)	98.62 (97.8)
Total reflections	170,172
Unique reflections	56,724
Refinement ($F > 0\ \sigma$)	
Resolution (Å)	50-2.4
R/R_{free} (%)[c]	23.4/28.7
Average B-factor (Å^2)	30.98
Number of protein atoms	9496
Number of water molecules	283
Number of phosphate ions	7
Root mean square deviation bonds (Å)	0.007
Root mean square deviation angles (°)	1.44

[a] The values for the highest shells are given in parentheses.
[b] $R_{sym} = \Sigma_h\Sigma_i|I_{h,i} - I_h|/\Sigma_h\Sigma_i I_{h,i}$, where I_h is the mean intensity of the *i* observations of symmetry related reflections of *h*.
[c] $r = \Sigma||F_o| - |F_c||/\Sigma|F_o|$, where $F_o = F_p$, and F_c is the calculated protein structure factor from the atomic model. R_{free} was calculated with 10% of the reflections.

RESULTS AND DISCUSSION

Inorganic Phosphate Induces DJ-1 Aggregation—Despite the existence of DJ-1 aggregates *in vivo*, recombinant DJ-1 was known to be a dimeric protein (11, 30–33). During efforts to obtain aggregated DJ-1, we were aware that brain cells of PD, multiple system atrophy, and Alzheimer disease patients where DJ-1 aggregation has been observed also contain elevated levels of inorganic phosphate, a vital molecule involved in almost all metabolic processes (34, 35). High P_i levels in serum are directly related to some diseases (36). Thus, we tested sodium phosphate buffers containing P_i to set an environment favorable for formation of DJ-1 aggregates, instead of Tris buffers, which had been previously used to purify recombinant DJ-1 (11). For easy, effective analysis of aggregation, we performed dynamic light scattering measurements. DJ-1 purified using sodium phosphate buffers (pDJ-1) exhibited a very interesting feature compared with DJ-1 purified using Tris buffers (tDJ-1). tDJ-1 showed a hydrodynamic radius (R_h) of 2.92 nm, representing the dimeric conformation with a molecular mass of ~40 kDa, whereas pDJ-1 had an R_h of 41.04 nm, a clear indication of aggregates (Fig. 1*A*). The pDJ-1 proteins purified with sodium phosphate buffers of different concentrations were subjected to dynamic light scattering to determine the effect of P_i concentration on DJ-1 aggregation. Interestingly, DJ-1 aggregates with large R_h were detected over 2 mM sodium phosphate buffers,

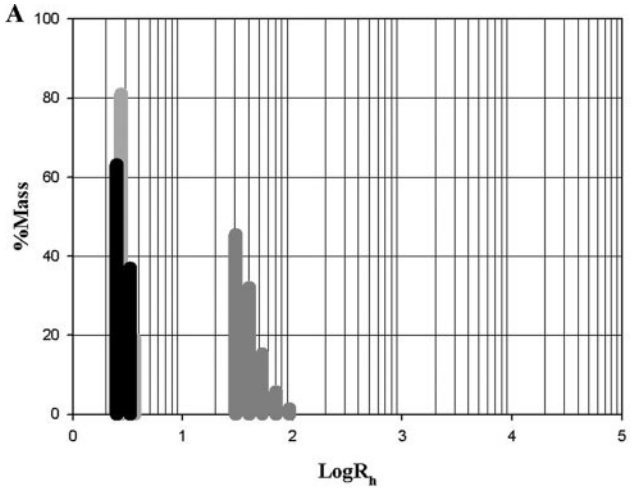

	Radius	Polyd	% Polyd	% Mass
tDJ-1 (gray)	2.92	0.35	12	99.9
pDJ-1 (dark gray)	41.04	13.04	31.8	100
R48A (black)	2.75	0.39	14	99.9

FIGURE 1. **The size distribution histograms from dynamic light scattering experiments and CD spectra.** *A*, histogram of tDJ-1, pDJ-1, and R48A. The table located below the size distribution histogram lists the number of peaks and their mean value (radius equal to R_h), polydispersity (*Polyd*), percentage of polydispersity (*%Polyd*), and estimated relative amount of mass (concentration) of each peak or species (*%Mass*). *B*, near-UV CD spectra of tDJ-1 (○) in 20 mM Tris buffer and pDJ-1 (●) in 50 mM sodium phosphate buffer. The final CD spectra were obtained by subtracting the spectra of the buffers from the spectra of the samples. Protein solutions with an OD of 0.66 at 280 nm were used for CD experiments.

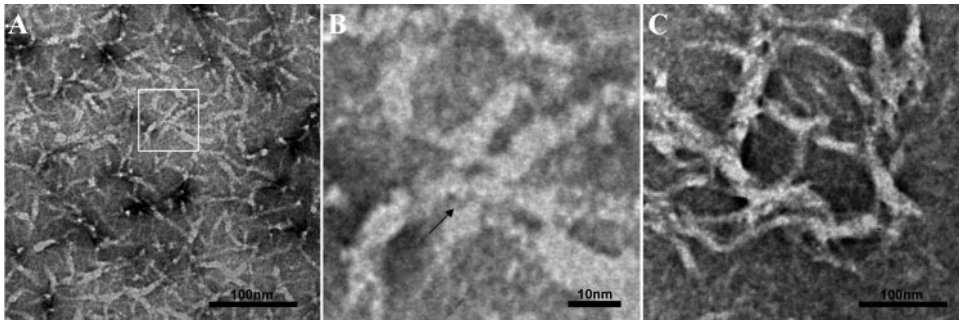

FIGURE 2. **Electron micrographs of DJ-1 filaments.** *A*, DJ-1 was negatively stained 1 day after purification and visualized. The thickness of protofilaments is 55–65 Å, which is similar to the 60 Å width of our structural model for protofilaments shown in Fig. 3*C*. *B*, the enlarged view of the *boxed region* in *A* contains protofilaments with their lateral contact marked by an *arrow*. *C*, filaments 2–5 times thicker than the protofilaments in *A* were observed when the sample was stained 3 days after purification.

which is a concentration comparable with the elevated P_i levels in the brains of PD patients (34, 35). We also observed time dependence of DJ-1 aggregation in buffers of low P_i concentration. Fresh pDJ-1 purified with 20–50 mM sodium phosphate buffers exhibited large R_h values. In contrast, fresh pDJ-1 in 2–10 mM sodium phosphate buffers exhibited R_h of the dimeric conformation; they showed large R_h values in a time-dependent manner. For example, pDJ-1 purified with a 2 mM sodium phosphate buffer began to display large R_h values 15 days after purification. It should be noted that tDJ-1 has the dimeric R_h value even 15 days after purification.

The structural differences between tDJ-1 and pDJ-1 are also reflected in a near-UV CD spectrum (Fig. 1*B*). The near-UV CD spectrum of a protein provides a valuable fingerprint of the tertiary structure of proteins, which can be used to compare protein structures (37).

Structural Investigation of DJ-1 Aggregates—To elucidate the structural property of DJ-1 aggregates, we employed electron microscopy. Because it takes a long time for pDJ-1 in buffers of low P_i concentration to form aggregates, we used pDJ-1 purified with a 50 mM sodium phosphate buffer for structural studies. Electron micrographs (EM) of pDJ-1 solutions were obtained on the first 3 days after purification. EM revealed that DJ-1 aggregates have a filamentous shape that gets longer and thicker with time (Fig. 2). The time dependence of DJ-1 aggregates is consistent with the dynamic light scattering results. The low resolution of EM limits structural information on DJ-1 filamentous aggregates. Thus, to obtain an atomic view of DJ-1 aggregates, we grew pDJ-1 crystals. The rod-shaped crystals of pDJ-1 exhibit a filamentous arrangement of DJ-1 molecules. Three DJ-1 dimers and one monomer, which are stacked, exist in an asymmetric unit. The monomer becomes a dimer via the 2-fold crystallographic symmetry. Consequently, continuous stacking of DJ-1 dimers is achieved, resulting in the formation of straight protofilaments (Fig. 3, *A* and *B*). Protofilaments are further packed in a side-by-side manner, organized in a filamentous assembly (Fig. 4*A*).

Within the protofilaments, DJ-1 dimers are piled in a rotational head-to-tail manner. The rotational axis of this conformation coincides with the protofilament axis (Fig. 3*A*), giving the protofilaments the appearance of circular cylinders when viewed from above (Fig. 4*A*). The top side of a DJ-1 dimer makes tight contact with the bottom side of the next dimer, displaying a ~103° (720°/7) rotational difference (Fig. 3*A*). As a result, the

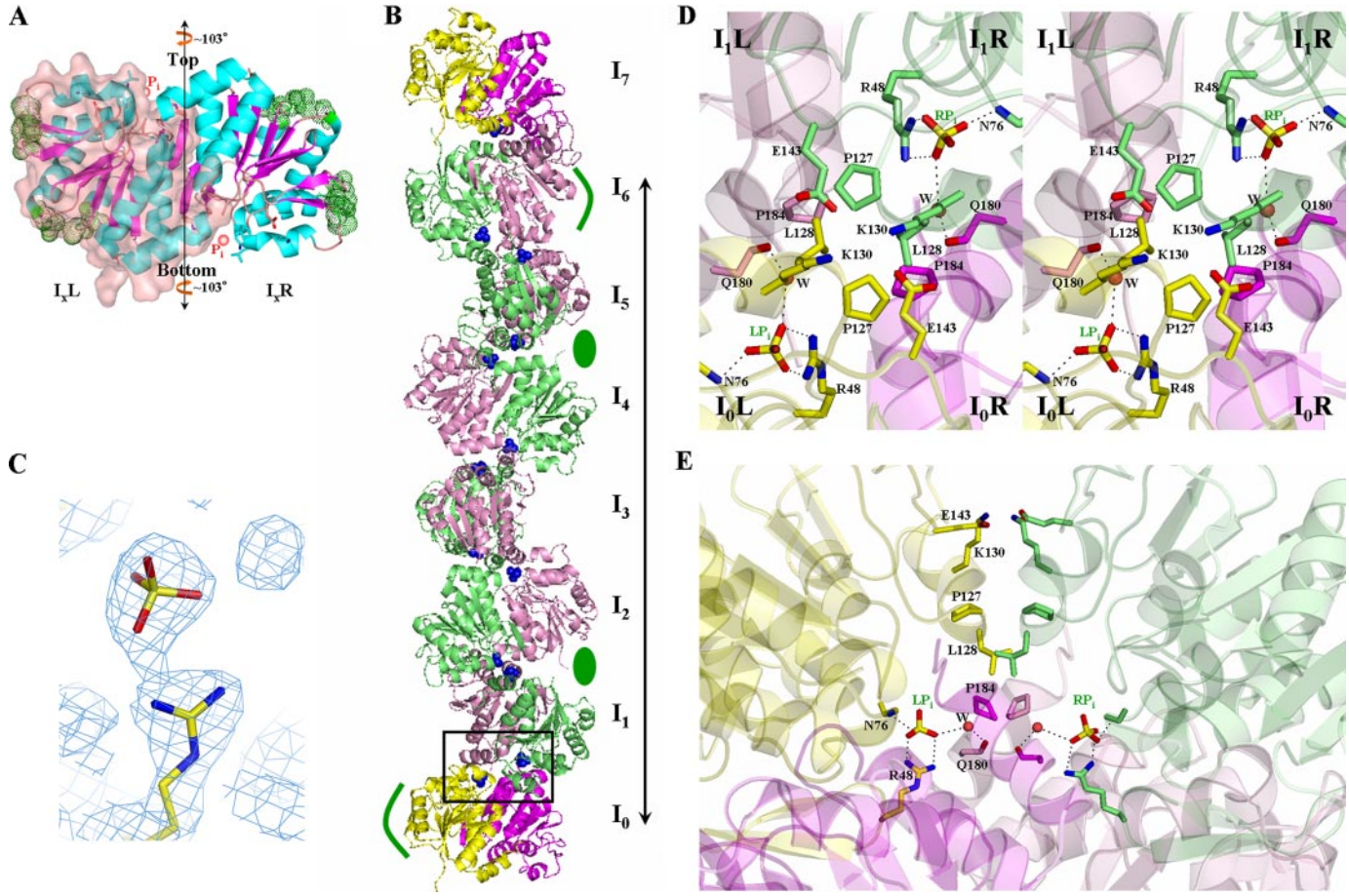

FIGURE 3. **Structure of DJ-1.** *A*, ribbon diagram of a DJ-1 dimer in the reference orientation. I_xL and I_xR stand for the left and right monomers of an I_x dimer in this orientation, respectively. To distinguish monomers in the dimer, I_xL is covered with transparent surface. The 2-fold axis is vertical to the figure. *Green dots* represent sites involved in lateral interactions, *sticks* represent residues implicated in the F contacts, and *red spheres* represent P_i. The *vertical line* with *arrows* at both ends represents the protofilament axis, that is, the rotational axis. *B*, ribbon drawing of a protofilament. I_{1-6}L and I_{1-6}R monomers are shown in *pink* and *lime*, respectively. For emphasis on the identity between I_0 and I_7 dimers, the two dimers are differently colored; the left and right monomers of I_0 and I_7 dimers are in *yellow* and *magenta*, respectively. The *long line* shows one longitudinal repeat unit of a protofilament. *Green ellipses* indicate the location of grooves involved in the lateral interactions between protofilaments, and *curved green lines* show the prominence regions. P_is are shown as *blue spheres*. The *boxed region* is the F interface between I_0 and I_1 dimers. The 2-fold axis of the F interface is *vertical* to the figure. *C*, the final $2F_o - F_c$ electron density map, contoured at 1 σ, showing Arg^{48} and an inorganic phosphate. *D*, front view of the *boxed region* of *B*. Residues implicated in the F contacts are labeled and represented by *sticks*. Oxygen, nitrogen, and sulfur atoms are shown in *red*, *blue*, and *yellow*, respectively. The color scheme for carbon atoms is identical to that in Fig. 1*B*. Polar interactions between atoms are shown as *dashed white lines*. *E*, side view of the boxed region of *B*. The color scheme for carbon atoms is identical to that in Fig. 1*B*.

I_7 dimer exhibits the same orientation as the I_0 dimer after 720° rotation; hence, the seven (from I_0 to I_6) dimers constitute one longitudinal repeat unit of DJ-1 protofilaments (Fig. 3*B*). No detectable structural differences were observed among the dimers stacked in the protofilaments. In addition, the dimers in the protofilaments are nearly structurally identical to free DJ-1 dimers (11); their backbone atoms align with an root mean square deviation of 0.175 Å. The contacts between dimers in the protofilaments, hereafter referred to as "F contacts," bury 1809 $Å^2$ of the solvent-accessible surface area of a DJ-1 dimer. A closer look at the F interfaces reveals their inherent 2-fold symmetry, as well as three major F contacts along the 2-fold axis: ion pairs, a hydrophobic core, and P_i-mediated contacts (Fig. 3, *D* and *E*). Because all of the F interfaces in protofilaments are identical, we describe only one F interface, which is located between the I_0 and I_1 dimers. Lys^{130} and Glu^{143} of the I_0L monomer form ion pairs with Glu^{143} and Lys^{130} of the I_1R monomer, respectively. Pro^{127} and Leu^{128} from the I_0L monomer and I_1R monomer, coupled with Pro^{184} from the I_0R and I_1L monomers, form the hydrophobic core. Two P_is, related by the F 2-fold axis, take positions at the F interface, mediating extensive contact: one is located between the I_0L and I_1L monomers (LP_i), and the other is located between the I_0R and I_1R monomers (RP_i) (Fig. 3, *C–E*). LP_i directly forms polar interactions with the guanidium group of Arg^{48} and the amide nitrogen of Asn^{76} in the I_0L monomer and makes a water-mediated hydrogen bond with the carbonyl oxygen of Gln^{180} in the I_1L monomer. RP_i is coordinated in an identical fashion. Because the guanidium group of Arg^{48} participates in coordinating P_i (Fig. 3, *C–E*), its elimination would prevent the binding of P_i at the F interfaces, affecting the formation of filamentous aggregates. To establish the role of P_i as an inducer of filamentous aggregates, we generated a R48A mutant. The mutant exhibits an R_h of 2.75 nm even in a high P_i concentration (Fig. 1*A*), pointing to the critical role of P_i in DJ-1 aggregation.

Protofilaments run parallel with one another in crystals. Although one protofilament is surrounded by six others, two of these do not actually contact the central protofilament (Fig. 4*A*,

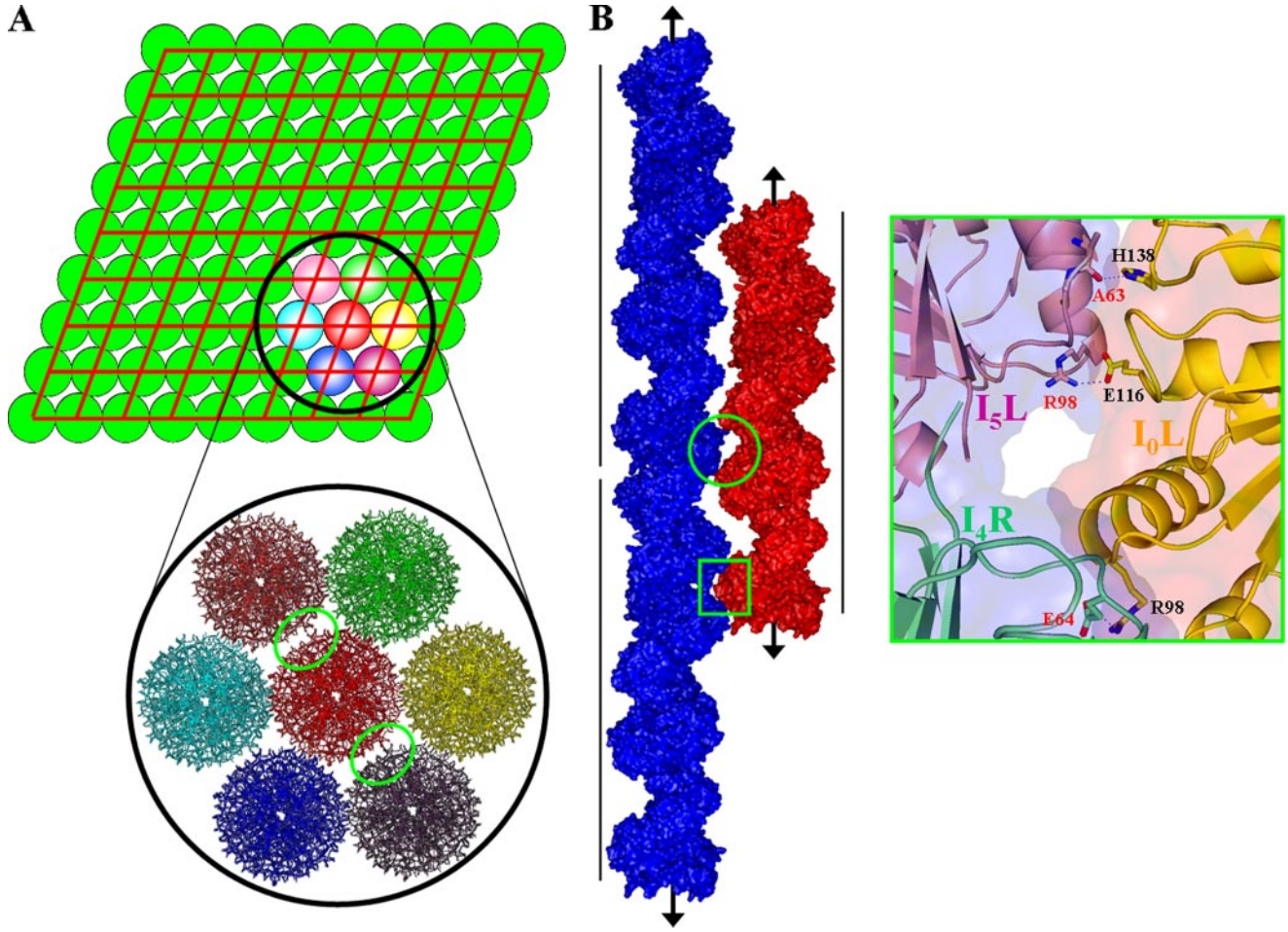

FIGURE 4. **Lateral arrangements among protofilaments.** *A, top*, schematic drawing of the top view. Each *circle* represents one protofilament, and *red lines* show the contacts between protofilaments. *Bottom*, packing model of seven protofilaments simulated in QUANTA. The *green ellipsoids* show that the central protofilament in red makes no contact with two neighboring protofilaments. *B*, *left panel*, surface representation showing a lateral contact between the central protofilament in *red* and the *blue* protofilament in *A*. The *three long lines* indicate the longitudinal repeat units of protofilaments, and the *four short arrows* represent the protofilament axes. The *green box* covers the only contact between the longitudinal repeat unit of the central protofilament and the adjacent protofilament in *blue*. There are no lateral interactions in the *green circle*, although slight contacts between protofilaments are seen because of the figure orientation. *Right panel*, the close-up view of the region covered by the *green box* in the *left figure*. The surfaces are transparently represented to show the interior. The residues implicated in the lateral interactions are represented by *sticks* and labeled. Oxygen and nitrogen are shown in *red* and *blue*, respectively. Polar interactions between atoms are shown as *dashed black lines*.

bottom panel), thus displaying a parallelogram pattern when viewed from the top (Fig. 4*A*, *top panel*). The lateral interactions between protofilaments exhibit good geometric complementarities, such that prominence regions in protofilaments fit into grooves in adjacent protofilaments (Fig. 4*B*). The I_0L and I_6L monomers function as prominences, and the grooves participating in these lateral interactions are located both between the I_1R and I_2L monomers and between the I_4R and I_5L monomers (Fig. 3*B*). Consequently, four lateral contact sites are located in each longitudinal repeat unit of a protofilament. Each site in a longitudinal repeat unit interacts with one of the surrounding protofilaments, and thus each longitudinal repeat unit makes contact with four protofilaments. The lateral interface between a prominence and a groove is composed of two contacting parts. Because all the lateral interfaces are identical, for convenience we describe only one lateral interface between the I_0L prominence of a protofilament and the groove between the I_4R and I_5L monomers of an adjacent protofilament. One component of the interface is formed by the contact between the I_0L prominence and the I_5L monomer of the groove (Fig. 4), where Glu^{116} and His^{138} of I_0L form ion pairs with Arg^{98} and the carbonyl carbon of Ala^{63} of I_5L in the groove, respectively. The other interface component is formed by the contact between the I_0L prominence and the I_4R monomer of the groove (Fig. 4). The only interaction occurring in the second component is the ion pairing between Arg^{98} of I_0L and Glu^{64} of I_4R in the groove. Compared with the F contacts, lateral contacts are not extensive. Lateral interactions between a prominence and a groove bury only 357 $Å^2$ of the solvent-accessible surface. This nonextensive lateral contact would allow DJ-1 to be assembled into a multitude of different aggregates through a different arrangement of lateral interactions, in the same manner as other filamentous proteins that form crystalline, curved, or branched aggregates (38, 39).

Comparison between EM and Crystal Structure—Although detailed comparisons between the EM and crystal structure are not possible because of the low resolution of the EM, the overall nature of the crystal structure seems to be well reflected in the EM. Similar to the protofilament structure (Fig. 3*B*), the EM protofilaments resemble the anterior view of a human spine, *i.e.*

a row of small bones (Fig. 2, *A* and *B*). The dimensions (~60 × ~50 Å) of the objects that correspond to small bones in the spine are comparable with those of DJ-1 dimers, representing the stacking of DJ-1 dimers in the protofilaments (Fig. 3*B*). In addition, the contact between protofilaments, which is marked by an *arrow* in Fig. 2*B*), is reminiscent of the aforementioned lateral interactions, exhibiting geometric complementarity between prominences and grooves (Fig. 4*B*).

Concluding Remarks—DJ-1 is implicated in PD pathogenesis (7), and insoluble DJ-1 aggregates have been observed in brains of patients with neurodegenerative diseases (24–29). Because protein aggregates not only are diagnostic hallmarks but have also been implicated in the pathogenesis of neurodegenerative diseases (40), physicochemical information on *in vivo* DJ-1 aggregates bears potential for further understanding of the etiology of PD. Here, we describe a biochemical and structural investigation of *in vitro* DJ-1 aggregates whose formation is dependent only on P_i. Unfortunately, there have been no reports on the characterization of *in vivo* DJ-1 aggregates, which precludes direct comparison between *in vivo* aggregates and the P_i-induced DJ-1 aggregates presented in this study. Therefore, we cannot assert that *in vivo* DJ-1 aggregates share characteristics with the P_i-induced aggregates. However, considering the observation that recombinant proteins forming pathological aggregates in brains can assemble into aggregates *in vitro* that closely resemble corresponding *in vivo* aggregates (41), the physicochemical properties of the P_i-induced aggregates might provide some insights into those of *in vivo* DJ-1 aggregates.

The loss of DJ-1 function induced by mutations in the *DJ-1* gene has been reported to lead to neurodegeneration (7). There is an emerging consensus that DJ-1 may provide protective roles against various stresses such as the oxidative damage involved in PD pathogenesis (22, 42–44). DJ-1 aggregation, which removes soluble DJ-1, would lead cells to lose functional DJ-1 that normally performs neuroprotective roles. As such, DJ-1 aggregation may be compatible with the loss-of-function pathogenic mechanism of DJ-1 (7). To determine the pathological role of the P_i-dependent DJ-1 aggregation, however, it is prerequisite to reveal the *in vivo* relationship between fragmentary observations of the P_i level and the DJ-1 aggregation. The increased P_i level in the brains of patients with neurodegenerative diseases (34, 35) shows that their physiological conditions can be thought to have been shifted to more suitable environments for DJ-1 aggregation. Nevertheless, because of the lack of any information on the cellular factors affecting protein aggregation, it is not certain that the observed DJ-1 aggregates *in vivo* (24–29) are correlated with the P_i level. It should also be noted that the P_i-dependent DJ-1 aggregation is described here for the first time. Consequently, at present we cannot determine whether P_i elevation induces DJ-1 aggregation in the brain, culminating in neurodegeneration. A future challenge is to address this issue.

Although the implication of the P_i-dependent DJ-1 aggregation in the pathogenesis of PD remains to be elucidated, the novel finding regarding the critical role of P_i in DJ-1 aggregation and the detailed view of a DJ-1 filamentous assembly at atomic resolution extends our knowledge of molecular mechanisms behind protein aggregation and provides an important framework for future works in unveiling the physiological meaning of the P_i-dependent DJ-1 aggregation.

REFERENCES

1. Nagakubo, D., Taira, T., Kitaura, H., Ikeda, M., Tamai, K., Iguchi-Ariga, S. M., and Ariga, H. (1997) *Biochem. Biophys. Res. Commun.* **231,** 509–513
2. Hod, Y., Pentyala, S. N., Whyard, T. C., and El-Maghrabi, M. R. (1999) *J. Cell. Biochem.* **72,** 435–444
3. Takahashi, K., Taira, T., Niki, T., Seino, C., Iguchi-Ariga, S. M., and Ariga, H. (2002) *J. Biol. Chem.* **276,** 37556–37563
4. Klinefelter, G. R., Laskey, J. W., Ferrell, J., Suarez, J. D., and Roberts, N. L. (1997) *J. Androl.* **18,** 139–150
5. Wagenfeld, A., Yeung, C. H., Strupat, K., and Cooper, T. G. (1998) *Biol. Reprod.* **58,** 1257–1265
6. Welch, J. E., Barbee, R. R., Roberts, N. L., Suarez, J. D., and Klinefelter, G. R. (1998) *J. Androl.* **19,** 385–393
7. Bonifati, V., Rizzu, P., van Baren, M. J., Schaap, O., Breedveld, G. J., Krieger, E., Dekker, M. C. J., Squitieri, F., Ibanez, P., Joosse, M., van Dongen, J. W., Vanacore, N., van Swieten, J. C., Brice, A., Meco, G., van Duijn, C. M., Oostra, B. A., and Heutink, P. (2003) *Science* **299,** 256–259
8. Miller, D. W., Ahmad, R., Hague, S., Baptista, M. J., Canet-Aviles, R., McLendon, C., Carter, D. M., Zhu, P. P., Stadler, J., Chandran, J., Klinefelter, G. R., Blackstone, C., and Cookson, M. R. (2003) *J. Biol. Chem.* **278,** 36588–36595
9. Moore, D. J., Zhang, L., Dawson, T. M., and Dawson, V. L. (2003) *J. Neurochem.* **87,** 1558–1567
10. Olzmann, J. A., Brown, K., Wilkinson, K. D., Rees, H. D., Huai, Q., Ke, H., Levey, A. I., Li, L., and Chin, L. S. (2004) *J. Biol. Chem.* **279,** 8506–8515
11. Lee, S. J., Kim, S. J., Kim, I. K., Ko, J., Jeong, C. S., Kim, G. H., Park, C., Kang, S. O., Suh, P. G., Lee, H. S., and Cha, S. S. (2003) *J. Biol. Chem.* **278,** 44552–44559
12. Shendelman, S., Jonason, A., Martinat, C., Leete, T., and Abeliovich, A. (2004) *PLoS Biol.* **2,** e362
13. Yang, Y., Gehrke, S., Haque, M. E., Imai, Y., Kosek, J., Yang, L., Beal, M. F., Nishimura, I., Wakamatsu, K., Ito, S., Takahashi, R., and Lu, B. (2005) *Proc. Natl. Acad. Sci. U. S. A* **102,** 13670–13675
14. Kim, R. H., Peters, M., Jang, Y., Shi, W., Pintilie, M., Fletcher, G. C., DeLuca, C., Liepa, J., Zhou, L., Snow, B., Binari, R. C., Manoukian, A. S., Bray, M. R., Liu, F. F., Tsao, M. S., and Mak, T. W. (2005) *Cancer Cell* **7,** 263–273
15. Junn, E., Taniguchi, H., Jeong, B. S., Zhao, X., Ichijo, H., and Mouradian, M. M. (2005) *Proc. Natl. Acad. Sci. U. S. A* **102,** 9691–9696
16. Meulener, M., Whitworth, A. J., Armstrong-Gold, C. E., Rizzu, P., Heutink, P., Wes, P. D., Pallanck, L. J., and Bonini, N. M. (2005) *Curr. Biol.* **15,** 1572–1577
17. Menzies, F. M., Yenisetti, S. C., and Min, K. T. (2005) *Curr. Biol.* **15,** 1578–1582
18. Goldberg, M. S., Pisani, A., Haburcak, M., Vortherms, T. A., Kitada, T., Costa, C., Tong, Y., Martella, G., Tscherter, A., Martins, A., Bernardi, G., Roth, B. L., Pothos, E. N., Calabresi, P., and Shen, J. (2005) *Neuron* **45,** 489–496
19. Kim, R. H., Smith, P. D., Aleyasin, H., Hayley, S., Mount, M. P., Pownall, S., Wakeham, A., You-Ten, A. J., Kalia, S. K., Horne, P., Westaway, D., Lozano, A. M., Anisman, H., Park, D. S., and Mak, T. W. (2005) *Proc. Natl. Acad. Sci. U. S. A* **102,** 5215–5220
20. Chen, L., Cagniard, B., Mathews, T., Jones, S., Koh, H. C., Ding, Y., Carvey, P. M., Ling, Z., Kang, U. J., and Zhuang, X. (2005) *J. Biol. Chem.* **280,** 21418–21426
21. Shinbo, Y., Niki, T., Taira, T., Ooe, H., Takahashi-Niki, K., Maita, C., Seino, C., Iguchi-Ariga, S. M., and Ariga, H. (2006) *Cell Death Differ* **13,** 96–108
22. Canet-Aviles, R. M., Wilson, M. A., Miller, D. W., Ahmad, R., McLendon, C., Bandyopadhyay, S., Baptista, M. J., Ringe, D., Petsko, G. A., and Cookson, M. R. (2004) *Proc. Natl. Acad. Sci. U. S. A* **101,** 9103–9108
23. Taira, T., Saito, Y., Niki, T., Iguchi-Ariga, S. M., Takahashi, K., and Ariga, H. (2004) *EMBO Rep.* **5,** 213–218
24. Neumann, M., Muller, V., Gorner, K., Kretzschmar, H. A., Haass, C., and

Kahle, P. J. (2004) *Acta Neuropathol.* (*Berl.*) **107,** 489–496
25. Rizzu, P., Hinkle, D. A., Zhukareva, V., Bonifati, V., Severijnen, L. A., Martinez, D., Ravid, R., Kamphorst, W., Eberwine, J. H., Lee, V. M., Trojanowski, J. Q., and Heutink, P. (2004) *Ann. Neurol.* **55,** 113–118
26. Baulac, S., LaVoie, M. J., Strahle, J., Schlossmacher, M. G., and Xia, W. (2004) *Mol. Cell Neurosci.* **27,** 236–246
27. Jin, J., Meredith, G. E., Chen, L., Zhou, Y., Xu, J., Shie, F. S., Lockhart, P., and Zhang, J. (2005) *Brain Res. Mol. Brain Res.* **134,** 119–138
28. Moore, D. J., Zhang, L., Troncoso, J., Lee, M. K., Hattori, N., Mizuno, Y., Dawson, T. M., and Dawson, V. L. (2005) *Hum. Mol. Genet.* **14,** 71–84
29. Moore, D. J., West, A. B., Dawson, V. L., and Dawson, T. M. (2005) *Annu. Rev. Neurosci.* **28,** 57–87
30. Tao, X., and Tong, L. (2003) *J. Biol. Chem.* **278,** 31372–31379
31. Wilson, M. A., Collins, J. L., Hod, Y., Ringe, D., and Petsko, G. A. (2003) *Proc. Natl. Acad. Sci. U. S. A* **100,** 9256–9261
32. Honbou, K., Suzuki, N. N., Horiuchi, M., Niki, T., Taira, T., Ariga, H., and Inagaki, F. (2003) *J. Biol. Chem.* **278,** 31380–31384
33. Huai, Q., Sun, Y., Wang, H., Chin, L. S., Li, L., Robinson, H., and Ke, H. (2003) *FEBS Lett.* **549,** 171–175
34. Barbiroli, B., Martinelli, P., Patuelli, A., Lodi, R., Iotti, S., Cortelli, P., and Montagna, P. (1999) *Mov. Disord.* **14,** 430–435
35. Brown, G. G., Levine, S. R., Gorell, J. M., Pettegrew, J. W., Gdowski, J. W., Bueri, J. A., Helpern, J. A., and Welch, K. M. (1989) *Neurology* **39,** 1423–1427
36. Dhingra, R., Sullivan, L. M., Fox, C. S., Wang, T. J., D'Agostino, R. B., Sr., Gaziano, J. M., and Vasan, R. S. (2007) *Arch. Intern Med.* **167,** 879–885
37. Kelly, S. M., Jess, T. J., and Price, N. C. (2005) *Biochim. Biophys. Acta* **1751,** 119–139
38. Lowe, J., and Amos, L. A. (1999) *EMBO J.* **18,** 2364–2371
39. Aebi, U., Fowler, W. E., Isenberg, G., Pollard, T. D., and Smith, P. R. (1981) *J. Cell Biol.* **91,** 340–351
40. Bucciantini, M., Giannoni, E., Chiti, F., Baroni, F., Formigli, L., Zurdo, J., Taddei, N., Ramponi, G., Dobson, C. M., and Stefani, M. (2002) *Nature* **416,** 507–511
41. Crowther, R. A., Jakes, R., Spillantini, M. G., and Goedert, M. (1998) *FEBS Lett.* **436,** 309–312
42. Batelli, S., Albani, D., Rametta, R., Polito, L., Prato, F., Pesaresi, M., Negro, A., and Forloni, G. (2008) *PLoS ONE* **3,** e1884
43. Yanagisawa, D., Kitamura, Y., Inden, M., Takata, K., Taniguchi, T., Morikawa, S., Morita, M., Inubushi, T., Tooyama, I., Taira, T., Iguchi-Ariga, S. M., Akaike, A., and Ariga, H. (2008) *J. Cereb Blood Flow Metab.* **28,** 563–578
44. Liu, F., Nguyen, J. L., Hulleman, J. D., Li, L., and Rochet, J. C. (2008) *J. Neurochem.*